Carbon 132 (2018) 598–605

Contents lists available at ScienceDirect

Carbon

journal homepage: www.elsevier.com/locate/carbon

Z-scheme Ag_3PO_4/graphdiyne/g-C_3N_4 composites: Enhanced photocatalytic O_2 generation benefiting from dual roles of graphdiyne

Hua-Yan Si [a, *], Chen-Jing Mao [a], Jin-Yuan Zhou [b], Xian-Feng Rong [b], Qi-Xin Deng [a], Shu-Lin Chen [d], Jin-Jin Zhao [a], Xiu-Guo Sun [a], Ying–Ming Shen [a], Wen-Jie Feng [c], Peng Gao [d], Jin Zhang [b]

[a] School of Materials Science and Engineering, Hebei Provincial Key Laboratory of Traffic Engineering Materials, Shijiazhuang Tiedao University, Shijiazhuang, 050043, China
[b] Center for Nanochemistry, Beijing Science and Engineering Center for Nanocarbons, Beijing National Laboratory for Molecular Sciences (BNLMS), College of Chemistry and Molecular Engineering, Peking University, Beijing, 100871, China
[c] Mechanics Engineering Department, Shijiazhuang Tiedao University, Shijiazhuang, 050043, China
[d] Electron Microscopy Laboratory, International Center for Quantum Materials, School of Physics, Peking University, Collaborative Innovation Centre of Quantum Matter, Beijing, 100871, China

ARTICLE INFO

Article history:
Received 11 December 2017
Received in revised form
27 February 2018
Accepted 28 February 2018
Available online 15 March 2018

ABSTRACT

Ag_3PO_4 nanoparticles are often considered to be a fascinating and efficient visible photocatalyst because of its high quantum efficiency and excellent activity of O_2 generation from water oxidation. However, the photo-corroded phenomenon and stability during the photocatalytic process reduce the photocatalytic activity. To overcome these disadvantages, strategies of combining Ag_3PO_4 with two-dimensional materials have been put forward to improve its stability and photocatalytic properties under visible-light irradiation. In this work, a novel Z-scheme Ag_3PO_4/graphdiyne/g-C_3N_4 nanocomposite was constructed via a simple electrostatic and π-π stacking interaction for the first time. Significantly, such Z-scheme nanostructures show highly oxygen evolution, and 753.1 μmol g^{-1} h^{-1} of O_2 was produced with Ag_3PO_4/graphdiyne/g-C_3N_4, which was 12.2 times higher than that of Ag_3PO_4 nanoparticles. Graphdiyne with π-conjugated structure of *sp*- and sp^2-hybridized carbon atoms, can not only act as conductive electron mediator bridges to collect photogenerated electrons and boost the O_2 evolution kinetics, but also used as a promising substrate for stabilizing Ag_3PO_4 in the composite.

1. Introduction

Solar water splitting over semiconductor photocatalysts has fascinated researchers recently due to its potential applications in renewable energy and environmental cleaning [1–3]. The development of novel and efficient semiconductors are highly demanded for direct water spitting. Basically, light absorption and suitable redox potentials are essential points. However, as semiconductors with suitable redox potentials are rare, a widely used strategy is to develop a composite photocatalytic system because of high charge-separation efficiency and strong redox ability. Compared to the proton reduction half-reaction in water splitting, the photocatalytic water oxidation reaction exhibits sluggish kinetics which limits the overall efficiency of water splitting [4]. Fortunately, Yi et al. reported that Ag_3PO_4 (APO) semiconductor showed high quantum efficiency and excellent activity of O_2 generation from water oxidation under visible light illumination [5]. However, the photo-corroded [6] phenomenon for APO reduces the photocatalytic activity and stability during the photocatalytic process. Up to now, strategies of combining APO with two-dimensional materials such as Ag_2S [7], graphene [8], rGO [9,10] and g-C_3N_4 [11–16] have been put forward to improve the stability and photocatalytic properties under visible-light irradiation. However, the heterostructures'low conjunction or agglomeration also limit the photo-induced charge separation. Therefore, it is still highly essential for improving the photocatalytic activity and stability of APO.

The artificial heterogeneous Z-scheme photocatalytic systems, mimicking the natural photosynthesis process, may overcome the aforementioned drawbacks. This is because an exceptional redox ability can be achieved in the Z-scheme photocatalytic system by

* Corresponding author.
E-mail address: dsscnewman@163.com (H.-Y. Si).

https://doi.org/10.1016/j.carbon.2018.02.107
0008-6223/

maintaining higher valence band and absolute value for conduction band potential, which also possesses relatively high separation efficiency of photogenerated carriers [17,18]. A typical Z-scheme is of two semiconductors and a solid electron mediator which can reduces the distance of Z-scheme electron transfer and avoid the backward reactions [18]. To date, many noble metals such as Au and Ag as solid electron mediators have been investigated [19–26]. Considering the sustainable development and cost, the exploration of an earth-abundant, low cost and highly efficient solid electron mediator is great challenge in the development of a Z-scheme photocatalytic system.

Graphdiyne (GDY) [27] has attracted tremendous attention as a new allotropic form of carbon nanomaterial with π-conjugated structure of *sp*- and sp^2-hybridized carbon atoms. According to the theoretical calculation, the electron and the hole mobility of GDY is about $2 \times 10^5\ cm^2\ V^{-1}\ s^{-1}$ [28] and $10^4\ cm^2\ V^{-1}\ s^{-1}$ [29] order of magnitude, respectively. The conductivity of GDY has been measured to be $2.516 \times 10^{-4}\ S\ m^{-1}$, similar to that of single crystal Si [28]. Unlike other conventional sp^2-hybridized carbon systems (such as graphene), the metal-free GDY has uniformly distributed pores [30–32], which provides numerous accessible active sites and improves effective mass transport [29,33]. The GDY also has a tunable bandgap in the range of 0.46–1.22 eV, which is an advantage of GDY over graphene for optoelectronic and photocatalytic applications [34]. As a result of its favorable electronic structure and good capability for transferring photoexcited electrons and holes, it has been the focus of extensive investigations in the field of catalysis [30,35–42]. We envisioned that GDY could be employed as solid electron mediator to construct a Z-scheme system for oxygen production. It is believed that GDYs can give rise to additional novel characteristics and branch out new direction for photocatalysis.

Recently, graphitic carbon nitride (g-C_3N_4, CN) has become a promising catalytic materials due to its moderate band gap ($E_g = 2.7$ eV), nontoxicity, photochemistry stability and low price [43]. The APO/CN composite has demonstrated high activity for oxygen production [44,45], CO_2 reduction [45], and dye degradation [23,46], which ascribes to the formation of an efficient Z-scheme system under illumination. Thus, it would be of great interest to select GDY as carbon bridge to construct the Z-scheme photocatalytic system, where APO and CN are chosen as the two semiconductors for photocatalytic reactions under visible light. Compared with pure APO, CN, and APO/CN, the APO/GDY/CN Z-scheme photocatalytic system exhibited apparently enhanced photocatalytic O_2 production activity and stability. Furthermore, the mechanisms of charge-separation and photocatalytic activity enhancement over the APO/GDY/CN Z-scheme photocatalytic system have been proposed.

2. Experimental section

2.1. Catalyst synthesis

2.1.1. Preparation of protonated CN nanosheet

In a typical procedure [47], bulk CN was obtained by heating of urea to 550 °C with a heating rate of 4.5 °C min^{-1}, and then the temperature was kept at 550 °C for 3 h. The bulk CN was milled in a mortar into powder and then transferred to a ceramic boat followed by an annealing process at 550 °C for 4 h with a ramp rate of 5 °Cmin^{-1}. The as-prepared CN nanosheet was pale yellow. The protonate CN nanosheets were prepared using previously reported method [48], this material (1 g) was vigorously stirred in HCl (25 mL, 10 M) for 1 h at room temperature. The mixture was filtrated and rinsed with deionized water several times. The protonated solid was put into deionized water and followed by sonicate-exfoliation for 2 h. The mixture was centrifuged at 3000 rpm to keep the suspension, denoted as CN nanosheets.

2.1.2. Preparation of APO

Dodecahedron APO were synthesized by a simple precipitation method [49]. CH_3COOAg (0.501 g) was dissolved in aqueous solution, Na_2HPO_4 (0.15 M) solution was added dropwise to the above solution, and golden yellow precipitation would be produced. The obtained samples were washed with water and dried at 60°Cin an oven.

2.1.3. Synthesis of GDY

GDY was synthesized on the copper foil by a cross-coupling reaction according to the Li's group method [28]. In brief, the monomer of hexaethynylbenzene was first synthesized by the reaction between tetrabutylammonium floride (TBAF) and hexakis [(trimethylsilyl)ethynyl]benzene in THF. In the presence of copper foil used as a catalyst for the cross-coupling reaction and substrate, the GDY was easily formed on the surface of copper foil by a cross-coupling reaction of the monomer of hexaethynylbenzene under a nitrogen atmosphere.

2.1.4. Preparation of APO/GDY/CN

Typically, GDY (1.0 mg) was dissolved in a solution of distilled water (10 mL) and ethanol (5 mL) by ultrasonic treatment for 1 h, and the as prepared g-C_3N_4 NSs (0.0023 g) was added to the obtained GDY solution. The mixed solution was stirred for another 2 h to achieve a homogeneous suspension. After CH_3COOAg (0.25 g) was added to above solution and stirred for another 30 min, Na_2HPO_4 solution (0.15 M) was dropwise added into the mixture under magnetic stirring. Finally, the resulting composite was centrifuged, rinsed with deionized water several times, and dried at 60 °C in vacuum. The APO/GDY/CN nanocomposites with different mass ratios of GDY (0, 0.03%, 0.04%, 0.05%,0.06%, 0.07%, 0.1%) were synthesized by varying the amounts of GDY and defined as APO/CN, APO-0.03%GDY-1%CN, APO-0.04%GDY-1%CN, APO-0.05%GDY-1%CN, APO-0.06%GDY-1%CN, APO-0.07%GDY-1%CN, and APO-0.1%GDY-1% CN. The pure Ag_3PO_4 and g-C_3N_4 were denoted APO and CN, respectively.

2.2. Characterization

The phase purity and crystal structure of the obtained samples were examined by X-ray diffraction (XRD, Bruker D8 Advance X-ray diffractometer) with Cu-Kα radiation (λ = 1.5406 Å). Infrared spectra were obtained on KBr pellets on a Nicolet NEXUS470 FTIR in the range of 4000-500 cm^{-1}. Field emission scanning electron microscopy (FESEM) measurement was performed by Hitachi S-4800 instrument. Transmission electron microscopy (TEM), scanning transmission electron microscopy (STEM) images and Energy dispersive X-Ray spectroscopy (EDX) mappings were acquired at an aberration-corrected FEI (Titan Cubed Themis G2) operated at 300 kV. Surface analysis of the sample was examined by X-ray photoelectron spectroscopy (XPS) using a Kratos Axis Ultra-DLD spectrometer. UV–vis diffuse reflectance spectra (DRS) were performed on a Hitachi U4100 spectrophotometer. Transient photocurrent and electrochemical impedance spectroscopy (EIS) measurements were performed on an electrochemical analyzer (CHI660E, CHI Shanghai, Inc.) in a standard three-electrode configuration using the as-prepared working electrodes as the working electrodes, a Pt plate as the counter electrode, and Hg/Hg_2Cl_2 (saturated KCl) as a reference electrode. A 300 W Xe arc lamp with a sharp cut-off filter served as a visible-light source (λ ≥ 420 nm). The working electrodes were prepared as follows: nanocomposites powder (5 mg) was added into ethanol (2 mL) and dispersed using ultrasonication for 30 min. Then, 200 μL of the

solution was dropped onto a 1 cm × 1.5 cm tin-oxide (ITO) glass substrate. Finally, the dried electrodes were calcined at 150 °C for 1 h in a N_2 gas flow.

2.3. Photocatalytic oxygen production

The photocatalytic oxygen production experiments were carried out in a 200 mL quartz flask at ambient temperature and atmospheric pressure, which was sealed with a silicone rubber septum. A 300 W xenon arc lamp with a 420 nm cutoff filter was used as an illumination source to trigger the photocatalytic reaction for the as-synthesized samples. During the O_2 evolution measurement, the illumination source was positioned 15 cm away from the quartz flask reactor. The focused illumination intensity on the flask was ca. 200 mW cm^{-2}. In a typical photocatalytic experiment, 10 mg of photocatalyst powder was dispersed in 80 mL aqueous solution. Before irradiation, the system was bubbled with nitrogen for 30 min to remove air and to ensure that the reaction system is under an inertial condition. The O_2 was analyzed by gas chromatography (GC 7900, 5 A molecular sieves column, TCD detector, Ar carrier) with the installed gas valve system. All the measurement conditions for O_2 production were kept the same to guarantee that the received results are comparable.

3. Results and discussion

As illustrated in Scheme 1, 2D CN nanosheets were first prepared by sonication/exfoliation of protonated CN. The protonated CN can afford CN nanosheets with a positively charged surface. The spontaneous assembly between the positively charged CN nanosheets and GDY with oxygen-containing functional groups (for example, COO^-) [14] was then achieved by electrostatic and π-π stacking interaction. Ag^+ was added into the above solution and self-assembled onto the surface of GDY. Following by HPO_4^{2-} treatment, APO/GDY/CN nanocomposite was successfully obtained.

Fig. 1 shows the X-ray diffraction (XRD) patterns of the CN, GDY, APO, and APO/GDY/CN nanocomposite, respectively. Pure APO is in the body-centered cubic structure (JCPDS No. 06-0505), while CN shows its characterization peaks at 27.4° and 13.0°, which can be indexed to the (002) and (100) diffraction planes of the graphite-like carbon nitride. The GDY pattern indicates that it is layered crystalline. All of the APO/GDY/CN nanocomposite diffraction peaks can be readily indexed to the body-centered cubic APO structure and no diffraction peaks of CN and any carbon species could be detected, which might be due to the low amount and relatively low diffraction intensity of CN and GDY.

The surface chemical composition and valence state of the APO/GDY/CN composite were studied systemically with XPS spectra shown in Fig. 2. The survey scan spectrum of APO/GDY/CN nanocomposite shows that APO/GDY/CN is mainly composed of element C, N, O, P and Ag (Fig. 2a). The high resolution of C 1s spectrum (Fig. 2b) can be deconvoluted into four main subpeaks corresponding to 284.80, 285.52, 286.61 and 288.50 eV, respectively. The main peak centered at 284.80 eV can be ascribed to the sp^2-hybridized carbon while the peak located at 285.52 eV is attributed to the *sp*-hybridized carbon. The peak located at 286.61 eV corresponds to C-O and that at 288.3 eV is related to C═O and C─N─C coordination. The evidence of *sp*-hybridized carbon atoms verifies that the model structure of GDY where the benzene rings connect to each other through the conjugated diyne links in GDY. Moreover, the corresponding high-resolution N 1s spectrum can be deconvoluted into three peaks at 399.01, 399.71, and 401.51 eV (Fig. 2c), which were corresponded to sp^2-hybridized (C═N-C), sp^3-hybridized nitrogen (N-$(C)_3$), and the terminal amino functional groups (C-N-H), respectively. All the results indicate the existence of the heptazine heterocyclic ring (C_6N_7) units, which are the elementary building blocks of CN. Two distinct peaks at 366.99 eV (Ag $3d_{5/2}$) and 374.25 eV (Ag $3d_{3/2}$) were also detected in the high-resolution Ag 3d spectrum (Fig. 2d) of APO/GDY/CN, which corresponds to Ag^+ in the composite.

Transmission electron microscopy (TEM) was used to further

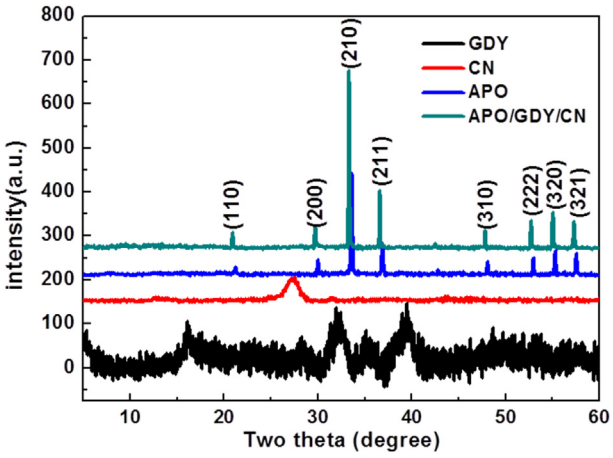

Fig. 1. XRD spectra of APO, GDY, CN, and APO/GDY/CN nanocomposite. (A colour version of this figure can be viewed online.)

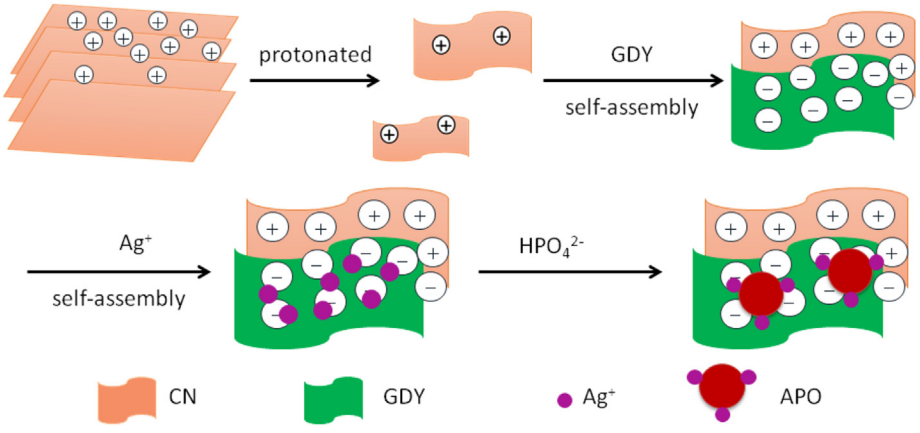

Scheme 1. Schematic of the preparation process of the APO/GDY/CN nanocomposite.

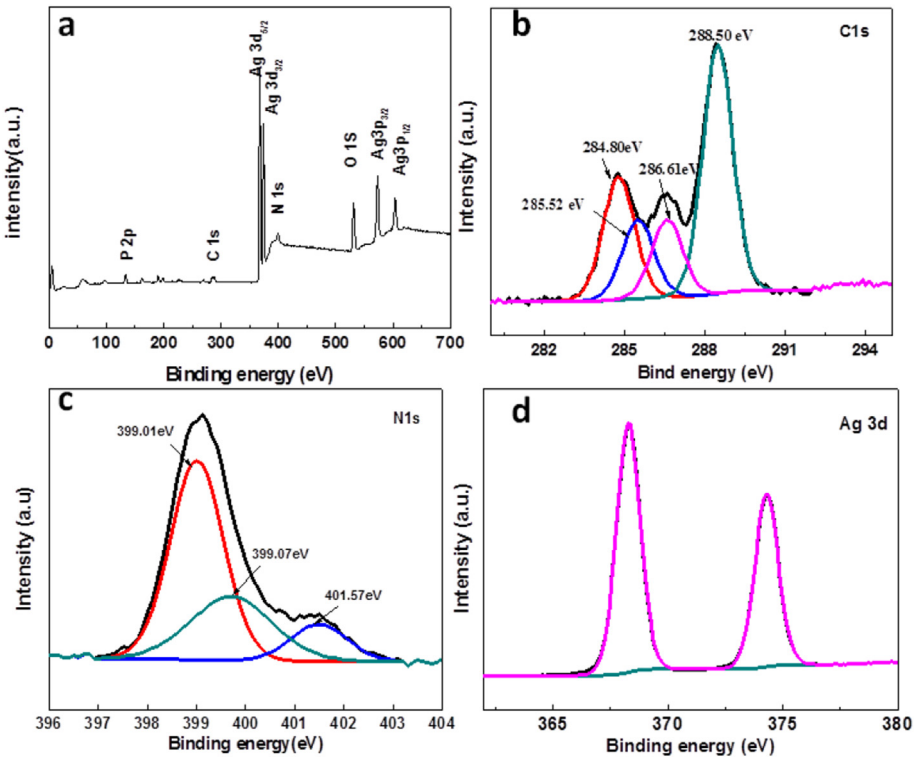

Fig. 2. (a) XPS survey spectra, (b–d) high-resolution XPS spectra of C 1s, N 1s and Ag 3d of APO/GDY/CN nanocomposite. (A colour version of this figure can be viewed online.)

characterize the morphologies and crystal phases. As shown in Fig. 3, the Ag_3PO_4 particles are regular rhombic dodecahedral morphology with an average diameter of 500 nm (Fig. 3a), and the dodecahedron Ag_3PO_4 was enclosed by 12 well-defined {110} planes which exhibit a higher surface energy than {100} facets [49]. The GDY nanosheet contains a layered structure with some silk-like fold. Corresponding selected area electron diffraction (SAED) patterns was shown in the inset of Fig. 3b and reveal the high crystallinity of GDY in certain areas. For the APO/GDY/CN samples (shown in Fig. 3c), it is clearly observed that the two-dimensional GDY/CN is well distributed in the composites, which has been clearly marked in the corresponding images. The high-resolution TEM images in Fig. 3d provide that the APO nanoparticles are in intimate contact with the GDY/CN, and the lattice fringes of APO have a spacing of 0.27 nm, which is in agreement with the spacing of the (210) planes of APO. It is noteworthy that there are no clear lattice-fringe spacings corresponding to the specific planes for CN and GDY nanosheets with a low degree of crystallinity, in conformity with the XRD result in Fig. 1. Moreover, the EDX elemental scanning analyses were also investigated. Fig. S1a–f showed the homogeneous distribution of Ag, P, O, C and N. The uniform distribution density of element C in the EDX mapping image is obvious much larger than that of element N, verifying that the GDY has been loaded on the surface of CN. Similarly, the element Ag exhibits higher density than element P in the same location (Figs. S1b and c), further demonstrating the coverage of APO nanoparticles on the surface of GDY/CN nanosheets. This result manifests direct evidence for the successful fabrication of the APO/GDY/CN nanocomposites.

The FT-IR spectra of CN, APO, GDY, CN/APO and APO/GDY/CN are shown in Fig. 4. Pure CN emerges several peaks in the range of 1200–1700 cm^{-1} ascribed to the typical stretching vibration of the C-N heterocycles. Furthermore, the peak at 806 cm^{-1} is attributed to the breathing mode of triazine units [50]. APO exhibits two peaks at 1008 and 551 cm^{-1}, which are attributed to the characteristic peaks of PO_4^{3-} [15] The peaks located at 1488 cm^{-1} and 1600 cm^{-1} in the as-grown GDY are assigned to the skeletal vibrations of aromatic ring, while the peak of 2050 cm^{-1} belongs to C≡C stretching vibration with slight the intensity due to the molecular perfectly symmetry [28]. Moreover, the FT-IR spectra of APO/GDY/CN composites represent the overlap of the characteristic peaks of all CN, GDY and APO.

Fig. 5 illustrates the UV–vis absorption spectra of the samples. As can be readily seen in Fig. 5a, the absorption edge of the CN is about 460 nm, and APO shows a broad absorption in the visible region from UV to the visible range up to 525 nm. The UV–vis absorption spectra of APO/GDY/CN composites has the strong absorption in the whole spectra of visible light range and the absorption intensity increases with the addition of GDY, which is the result of the excellent visible light absorption of GDY [29,35]. The higher absorption intensity of the APO/GDY/CN catalyst indicated that it might possess better photocatalytic performance.

The photocatalytic O_2 production activities of as-prepared photocatalysts were further investigated. Fig. 6 presents the photocatalytic O_2-production activities of samples without sacrificial reagent under visible-light irradiation ($\lambda \geq 420$ nm). No O_2 was detected under the nonirradiation or no photocatalysts, thus indicating that water is indeed oxidized upon light irradiation. For comparison purposes, the performance of bare CN, APO and CN/APO for O_2 was firstly measured under identical conditions. As shown in Fig. 6a, the CN sample shows a negligible O_2 evolution activity possibly due to a fast recombination of photocatalytic electron–hole pairs, and the O_2 evolution rate of APO and APO/CN are 61.4 and 375 μmol g^{-1} ·h^{-1}, respectively. In contrast, the average photocatalytic O_2 evolution rates over ternary APO/GDY/CN nanocomposites are found to be 379.2, 484.4, 753.1, 496.8, 485.5, 418.5 and 372.3 μmol g^{-1} h^{-1} for APO-0.03%GDY-1%CN, APO-0.04%GDY-1%CN, APO-0.05%GDY-1%CN, APO-0.06%GDY-1%CN, and APO-

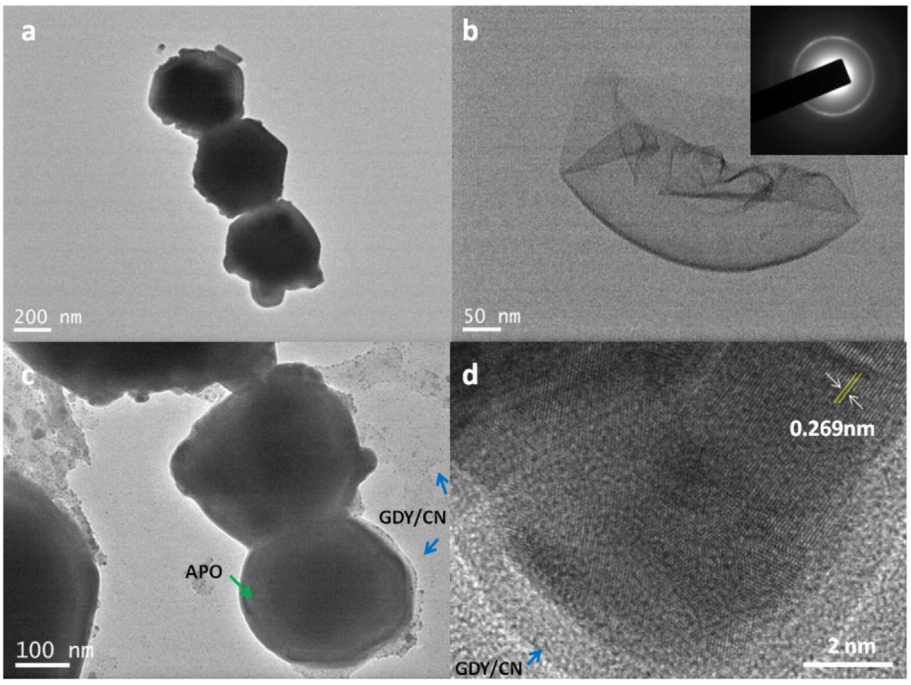

Fig. 3. TEM images of (a) APO, (b) GDY, (c) APO/GDY/CN and(d) HRTEM image of APO/GDY/CN. (A colour version of this figure can be viewed online.)

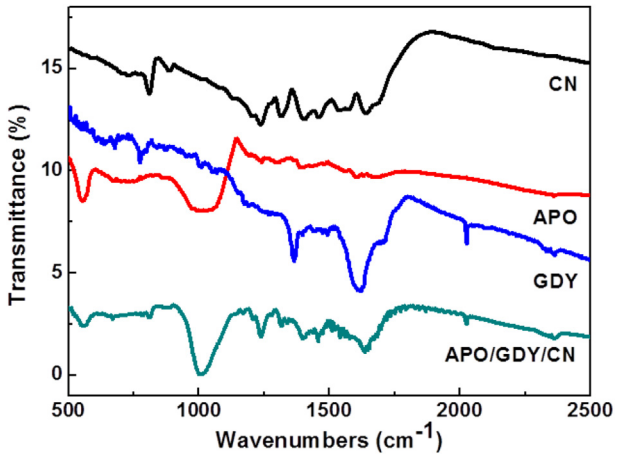

Fig. 4. FTIR spectra of APO, GDY, CN and APO/GDY/CN. (A colour version of this figure can be viewed online.)

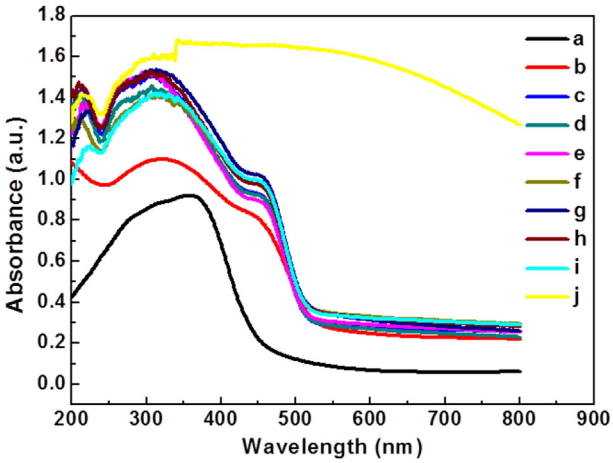

Fig. 5. UV–vis absorbance of (a) CN, (b) APO, (c) APO/CN, (d) APO-0.03%GDY-1%CN, (e) APO-0.04%GDY-1%CN, (f) APO-0.05%GDY-1%CN, (g) APO-0.06%GDY-1%CN, (h) APO-0.07%GDY-1%CN, (i) APO-0.1%GDY-1%CN and (j) GDY. (A colour version of this figure can be viewed online.)

0.07%GDY-1%CN, respectively. Obviously, with the increasing of the GDY mass ratio, the O_2 evolution activity increases greatly up to 0.05% (the O_2 evolution rates is 753.1 μmol g^{-1} h^{-1}, which is nearly12.2 and 2 times higher than that of APO and APO/CN, respectively). The vigorous bubbles of O_2 were being observed for APO-0.05%GDY-1%CN when light irradiation commenced (supplementary Movie S1). However, when the amount of GDY is higher than 0.05%, the O_2 evolution activity of the APO/GDY/CN composites decreases gradually. Compared with CN and APO, APO/CN, APO/GDY/CN composites (0.03%–0.1%) exhibit excellent O_2 evolution activity.

Supplementary data related to this article can be found at https://doi.org/10.1016/j.carbon.2018.02.107.

Impressively, the photocatalytic activity of APO/GDY/CN composites exhibits quite good stability even over 12 h operation as demonstrated in Fig. 6b. After three successive reaction cycles, no noticeable deactivation in the oxygen evolution can be found. A slight degradation in the photocatalytic activity is observed after 12 h. However, the recycling stability for APO/CN is not a patch on APO/GDY/CN composites, which reduce it to less than 86% after three cycles. However, After the next two successive reaction cycles, there are noticeable deactivation in the oxygen evolution. The APO/GDY/CN composites reduce it less than 6% while APO/CN there is nearly no O_2 emerged after 20 h. The good photocatalytic activity from such ternary nanostructures may be related to GDY, which can not only act as conductive electron mediator bridges to collect photogenerated electrons and boost the O_2 evolution kinetics, but also used as a promising substrate for stabilizing Ag^+ in the composite [35].

EIS and transient photocurrent experiments are effective means

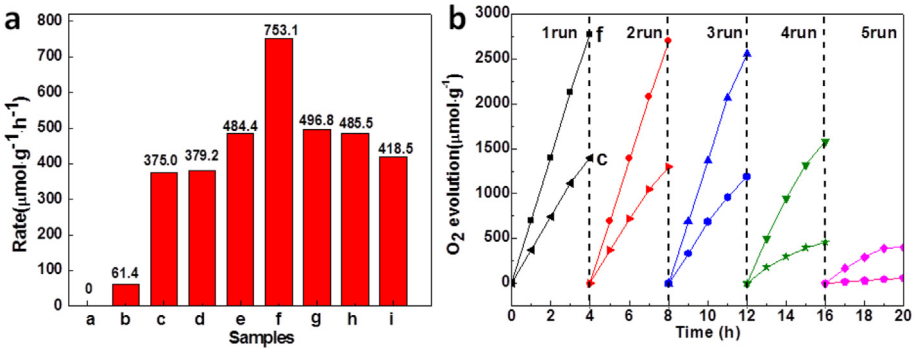

Fig. 6. (a) Average rate of O_2 evolution over different photocatalysts (a) CN, (b) APO, (c) APO/CN, (d) APO-0.03%GDY-1%CN, (e) APO-0.04%GDY-1%CN, (f) APO-0.05%GDY-1%CN, (g) APO-0.06%GDY-1%CN, (h) APO-0.07%GDY-1%CN, and (i) APO-0.1%GDY-1%CN, and (b) repeated time courses of photocatalytic O_2 evolution on samples (c) and (f). Reaction conditions: catalyst, 0.2 g; 120 mL distilled water; light source, xenon lamp (300 W) with a UV cut-off filter ($\lambda \geq 420$ nm). (A colour version of this figure can be viewed online.)

of investigating the improved charge separation and transfer efficiencies caused by the strong interface interaction between APO and GDY co-catalysts. Fig. 7ashows the EIS changes of CN, APO, APO/CN, and APO/GDY/CN electrodes. In general, the smaller arc in an EIS Nyquist plot indicates a slower recombination and a more efficient separation of photogenerated electron −hole pairs. The data in Fig. 7a shows that relative arc sizes for the nine electrodes are in the following order: f < g < h < e < i < d < c < j < b ≪a. This indicates that the APO/GDY/CN composite has the highest improvements of charge-separation efficiencies. The identical result was obtained using a transient photocurrent responses experiment. As shown in Fig. 7b, it is obvious that the ternary composite photocatalysts exhibit higher photocurrent density, and the f sample is 8.35 times, 16.7 times and 20.8 times higher than APO/CN、APO and CN, respectively. This further demonstrates that APO/GDY/CN is superior to APO/CN、APO or CN in separating electron−hole pairs, which are in good agreement with the highest O_2 evolution activity, confirming the outstanding roles of GDY in improving charge separation and transfer. It is worth noticing that photocatalytic activity would decrease when GDY amount was less than or more than 0.5%. The reason that GDY content has an effect on photocatalytic efficiency may be attributed to agglomeration due to its low solubility. This could lead to unfavourable effect on charge separation/transport in the active layer, which similar to carbon materials in the solar cells systems [51,52]. When the GDY content was low, the sufficient conductive electron mediator bridges could not be formed, which might restrict the separation of photoexcited electrons and holes.

To understand the photocatalytic mechanism over APO/GDY/CN composites, we studied the generation of active radicals involved in the photocatalytic system by the ESR in situ characterizations of the illuminated APO/GDY/CN composites with 5,5-dimethyl-1-pyrroline-N-oxide (DMPO) in methanol and water, respectively. As shown in Figure 8a, it can be seen that the characteristic peaks of the DMPO-•O_2^- adducts are observed over APO/GDY/CN and CN compared with APO under visible light irradiation, attributed to reduction of O_2 to •O_2^- since their CB potential of CN is more negative than $E_0(O_2/•O_2^-)$ (−0.33 eV vs. NHE, as shown in Figure 9) [14], while there is no formation of •O_2^- for APO and blank. Moreover, the intensities of the DMPO-•O_2^- peaks over APO/GDY/CN are higher than that over CN, indicating that more •O_2^- are generated over APO/GDY/CN than CN. In Figure 8b, APO/GDY/CN and APO all have characteristic peaks DMPO-•OH ascribed to the holes on the VB of APO oxidizing OH^- to •OH, since its VB potential is more positive than $E_0(OH^-/•OH)$. The intensity of the DMPO-•OH adduct from APO/GDY/CN is higher than that of the APO one. In addition, there are no DMPO-•OH signals for CN and blank.

On the basis of the above experimental evidence, the possible photocatalytic mechanisms of ternary APO/GDY/CN nanocomposites for OER have been proposed. From the thermodynamic limitations, only holes from the APO can generate •OH radicals because of their strong oxidation potential and only electrons from the CN can produce •O_2^- radicals due to their strong reduction potential under illumination (Figure 9). In the construction of a conventional semiconductor heterojunctions (Figure 9b), the expected charge separation and transfer are usually governed by the thermodynamics driving force, where the electrons in the CB of CN move to the CB of APO and holes in the VB of APO shift to the VB of

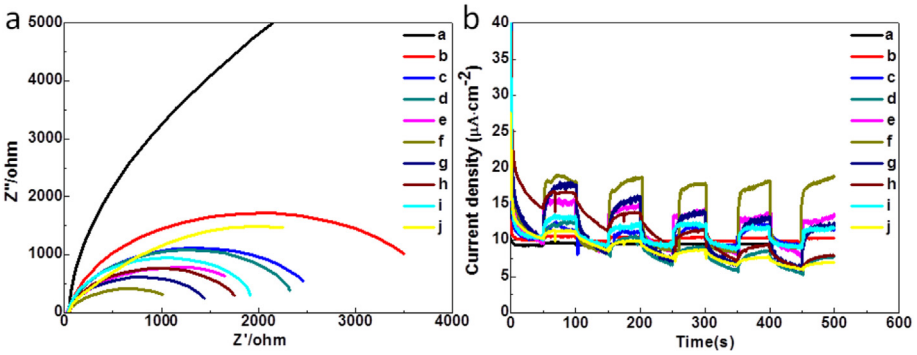

Fig. 7. (a) Electrochemical impedance spectroscopy and (b) transient photocurrent response for (a) CN, (b) APO, (c) APO/CN, (d) APO-0.03%GDY-1%CN, (e) APO-0.04%GDY-1%CN, (f) APO-0.05%GDY-1%CN, (g) APO-0.06%GDY-1%CN, (h) APO-0.07%GDY-1%CN, (i) APO-0.1%GDY-1%CN and (j) GDY samples, respectively. (A colour version of this figure can be viewed online.)

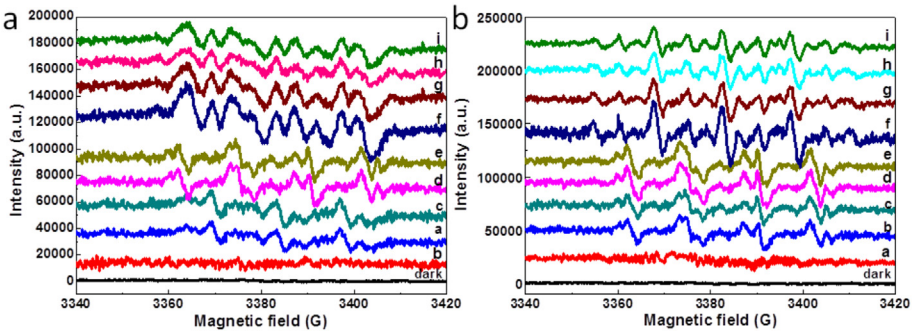

Fig. 8. ESR signals of (a) DMPO-•O_2^- and (b) DMPO-•OH with irradiationfor 30 s in methanol and aqueous dispersion, respectively. (a) CN, (b) APO, (c) APO/CN, (d) APO-0.03%GDY-1%CN, (e) APO-0.04%GDY-1%CN, (f) APO-0.05%GDY-1%CN, (g) APO-0.06%GDY-1%CN, (h) APO-0.07%GDY-1%CN, and (i) APO-0.1%GDY-1%CN. (A colour version of this figure can be viewed online.)

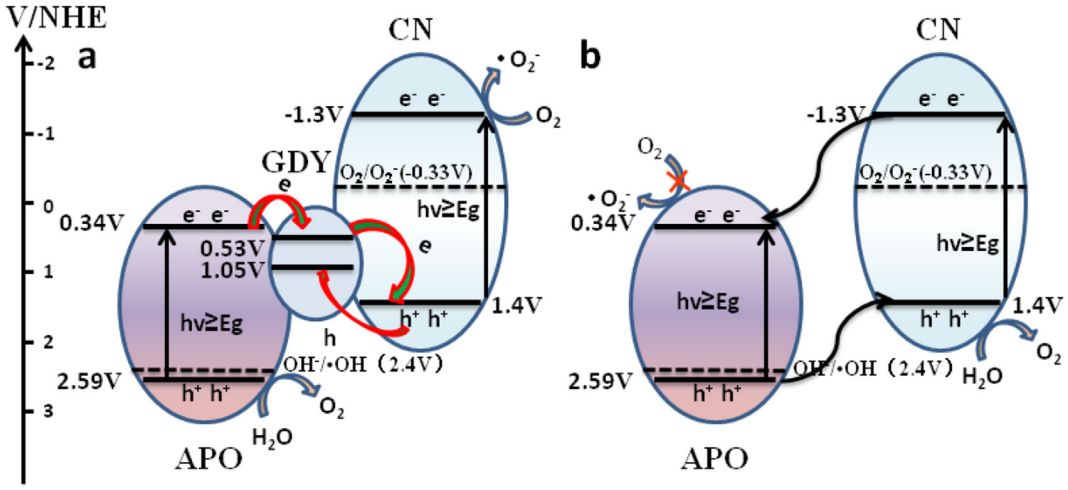

Fig. 9. Possible electron transfer mechanisms of (a) the APO/GDY/CN Z-scheme system and (b) the APO/CN heterojunction structure. (A colour version of this figure can be viewed online.)

CN. Either the reduction of O_2 to •O_2^- or the oxidation of OH^- to •OH becomes practically impossible because of the weak energetic driving force in this scenario [16]. Therefore, the charge-transfer mechanism of the APO/GDY/CN composite should be illustrated as in Figure 9a, when the GDY is added, due to the suitable band potentials [37], high surface area (Fig. S2), good visible-light responsive ability [35] and conductivity [28], the GDY could not only enhance the light absorption performance of the photocatalyst, but also act as the conducting medium to improve the transfer rates of both electron [30,35] and hole [37,41] in APO/GDY/CN. As a consequence, the conduction band (CB) electrons (photo-induced) transferred from APO to GDY, subsequently react with the valence band (VB) holes of CN mainly via the Z-scheme pathway (electron transfer, APO → GDY → CN) due to short charge transfer distance, which contributed to improve the charge separation [53]. Besides, the VB holes of CN may be injected to the VB of GDY simultaneously because of GDY's high hole mobility [41]. Thus, the electrons and holes would be accumulated in the CB of CN and VB of APO, respectively, inhibiting the recombination in both CN and APO. The holes in the VB of APO have superior oxidation, therefore leading to the improvement of photocatalytic O_2 production activity of the APO/GDY/CN nanocomposite.

In summary, this work demonstrated that the GDY could be used as the electron mediator to construct a novel APO/GDY/CN Z-scheme photocatalytic system. Compared with the APO, CN, and APO/CN heterojunction structure, the Z-scheme system significantly boost the O_2 evolution activity and stability due to its excellent charge separation and transfer efficiency. With the cost-effective process and high catalytic efficiency, this type of GDY-based Z-scheme system promises a new insight into multi-heterostructured composite photocatalysts for a wide range of applications.

Acknowledgements

The Project Sponsored by the Scientific Research Foundation for the Returned Overseas Hebei Province (C2013001055), Natural Science Foundation of Hebei Education Department (QN2015220), the National Nature Science Foundation of Hebei Province (B2016210111), the Training Program for Leading Talent in University Innovative Research Team in Hebei Province (LJRC006), and State Education Ministry and Hebei Key Discipline Construction Project. This work was also supported by the Ministry of Science and Technology of China (2016YFA 0200101 and 2016YFA0200104) and the National Natural Science Foundation of China (51432002, 21129001, 21233001, 51502007, 51672007). The authors acknowledge Electron Microscopy Laboratory in Peking University for the use of Cs corrected electron microscope.

Appendix A. Supplementary data

Supplementary data related to this article can be found at

https://doi.org/10.1016/j.carbon.2018.02.107.

References

[1] A. Fujishima, K. Honda, Nature 238 (1972) 37.
[2] C.L. Wang, D. Astruc, Chem. Soc. Rev. 43 (2014) 7188.
[3] Z. Zou, J. Ye, K. Sayama, H. Arakawa, Nature 414 (2001) 625.
[4] M.W. Kanan, D.G. Nocera, Science 321 (2008) 1072.
[5] Z.G. Yi, J.H. Ye, N. Kikugawa, T. Kako, S.X. Ouyang, H. Stuart-Williams, et al., Nat. Mater. 9 (2010) 559.
[6] C. Cui, Y.P. Wang, D.Y. Liang, W. Cui, H.H. Hu, B.Q. Lu, et al., Appl. Catal. B Environ. 158–159 (2014) 150.
[7] P.Y. Ma, H.J. Yu, Y. Yu, W.M. Wang, H. Wang, J.Y. Zhang, et al., Phys. Chem. Chem. Phys. 18 (2016) 3638.
[8] Q.J. Xiang, D. Lang, T.T. Shen, F. Liu, Appl. Catal. B Environ. 162 (2015) 196.
[9] A. Samal, D.P. Das, K.K. Nanda, B.K. Mishra, J. Das, A. Dash, Chem. Asian J. 11 (2016) 584.
[10] P.Y. Dong, Y.H. Wang, B.C. Cao, S.Y. Xin, L.N. Guo, J. Zhang, et al., Appl. Catal. B Environ. 132–133 (2013) 45.
[11] H. Katsumata, T. Sakai, T. Suzuki, S. Kaneco, Ind. Eng. Chem. Res. 53 (2014) 8018.
[12] L. Liu, Y.H. Qi, J.R. Lu, S.L. Lin, W.J. An, Y.H. Liang, et al., Appl. Catal. B Environ. 183 (2016) 133.
[13] N.N. Wang, Y. Zhou, C.H. Chen, L.Y. Cheng, H.M. Ding, Catal. Commun. 73 (2016) 74.
[14] J.F. Zhang, J.L. Lv, K. Dai, Q. liu, C.H. Liang, G.P. Zhu, Ceram. Int. 43 (2017) 1522.
[15] Y.M. He, L.H. Zhang, B.T. Teng, M.H. Fan, Environ. Sci. Technol. 49 (2015) 649.
[16] S.G. Meng, X.F. Ning, T. Zhang, S.F. Chen, X.L. Fu, Phys. Chem. Chem. Phys. 17 (2015) 11577.
[17] K. Maeda, ACS Catal. 3 (2013) 1486.
[18] P. Zhou, J.G. Yu, M. Jaroniec, Adv. Mater. 26 (2014) 4920.
[19] X.L. Zhang, Y. Li, J.L. Zhao, S.G. Wang, Y.D. Li, H.T. Dai, et al., J. Power Sources 269 (2014) 466.
[20] X.F. Wang, S.F. Li, Y.Q. Ma, H.G. Yu, J.G. Yu, J. Phys. Chem. C 115 (2011) 14648.
[21] N. Srinivasan, E. Sakai, M. Miyauchi, ACS Catal. 6 (2016) 2197.
[22] X.P. Xiao, J.H. Wei, Y. Yang, R. Xiong, C.C. Pan, J. Shi, ACS Sustain. Chem. Eng. 4 (2016) 3017.
[23] X.X. Li, T. Wan, J.Y. Qiu, H. Wei, F.H. Qin, Y.H. Wang, et al., Appl. Catal. B Environ. 217 (2017) 591.
[24] D.D. Zheng, C.Y. Pang, X.C. Wang, Chem. Commun. 51 (2015) 17467.
[25] H. Tada, T. Mitsui, T. Kiyonaga, T. Akita, K. Tanaka, Nat. Mater. 5 (2006) 782.
[26] H.J. Yun, H. Lee, N.D. Kim, D.M. Lee, S. Yu, J. Yi, ACS Nano 5 (2011) 4084.
[27] J.Y. Li, L. Xu, H.B. Liu, Y.L. Li, Chem. Soc. Rev. 43 (2014) 2572.
[28] G.X. Li, Y.L. Li, H.B. Liu, Y.B. Guo, Y.J. Li, D.B. Zhu, Chem. Commun. 46 (2010) 3256.
[29] M.Q. Long, L. Tang, D. Wang, Y.L. Li, Z.G. Shuai, ACS Nano 5 (2011) 2593.
[30] N. Yang, Y. Liu, H. Wen, Z. Tang, H. Zhao, Y. Li, et al., ACS Nano 7 (2013) 1504.
[31] X. Gao, X. Shen, Carbon 125 (2017) 536.
[32] Y. Tang, H. Yang, P. Yang, Carbon 117 (2017) 246.
[33] X. Qian, H. Liu, C. Huang, S. Chen, L. Zhang, Y. Li, et al., Sci. Rep. 5 (2015) 7756.
[34] Q. Peng, A.K. Dearden, J. Crean, L. Han, S. Liu, X. Wen, et al., Sci. Appl. 7 (2014) 1.
[35] S. Wang, L.X. Yi, J.E. Halpert, X.Y. Lai, Y.Y. Liu, H.B. Cao, et al., Small 8 (2012) 265.
[36] H.T. Qi, P. Yu, Y.X. Wang, G.C. Han, H.B. Liu, Y.P. Yi, et al., J. Am. Chem. Soc. 137 (2015) 5260.
[37] J. Li, X. Gao, B. Liu, Q.L. Feng, X.B. Li, M.Y. Huang, et al., J. Am. Chem. Soc. 138 (2016) 3954.
[38] Y.R. Xue, Y. Guo, Y.P. Yi, Y.J. Li, H.B. Liu, D. Li, et al., Nano Energy 30 (2016) 858.
[39] Y. Xue, J. Li, Z. Xue, Y. Li, H. Liu, D. Li, et al., ACS Appl. Mater. Interfaces 8 (2016) 31083.
[40] Y.R. Xue, Z.C. Zuo, Y.J. Li, H.B. Liu, Y.L. Li, Small 13 (2017), 1700936.
[41] Y.Y. Han, X.L. Lu, S.F. Tang, X.P. Yin, Z.W. Wei, T.B. Lu, Adv. Energy Mater. (2018), https://doi.org/10.1002/aenm.201702992.
[42] Y. Yao, Z.W. Jin, Y.H. Chen, Z.F. Gao, J.Q. Yan, H.B. Liu, et al., Carbon 129 (2018) 228.
[43] X.C. Wang, K. Maeda, A. Thomas, K. Takanabe, G. Xin, J.M. Carlsson, et al., Nat. Mater. 8 (2009) 76.
[44] X.F. Yang, H. Tang, J.S. Xu, M. Antonietti, M. Shalom, Chem. Sustain. Chem. 8 (2015) 350.
[45] X.F. Yang, Z.P. Chen, J.S. Xu, H. Tang, K.M. Chen, Y. Jiang, ACS Appl. Mater. Interfaces 7 (2015) 15285.
[46] S. Kumar, T. Surendar, A. Baruah, V. Shanker, J. Mater. Chem. A 1 (2013) 5333.
[47] F. Dong, Z.Y. Wang, Y.J. Sun, W.K. Ho, H.D. Zhang, J.Colloid. Interf. Sci. 401 (2013) 70.
[48] T.Y. Ma, S. Dai, M. Jaroniec, S.Z. Qiao, Angew. Chem. Int. Ed. 53 (2014) 7281.
[49] Y.P. Bi, S.X. Ouyang, N. Umezawa, J.Y. Cao, J.H. Ye, J. Am. Chem. Soc. 133 (2011) 6490.
[50] S. Kumar, T. Surendar, A. Baruahb, V. Shanker, J. Mater. Chem. A 1 (2013) 5333.
[51] H. Du, Z. Deng, Z. Lü, Y. Yin, L. Yu, H. Wu, et al., Synth. Met. 161 (2011) 2055.
[52] R.D. Costa, S. Feihl, A. Kahnt, S. Gambhir, D.L. Officer, G.G. Wallace, et al., Adv. Mater. 25 (2013) 6513.
[53] X. Yu, X.L. Fan, L. An, G.B. Liu, Z.H. Li, J.W. Liu, et al., Carbon 128 (2018) 21.